Research Article Vol. 6, No. 2 / February 2019 / Optica 206

Sub-milliwatt-level microresonator solitons with extended access range using an auxiliary laser

Shuangyou Zhang,[1] Jonathan M. Silver,[1,2] Leonardo Del Bino,[1,3] Francois Copie,[1] Michael T. M. Woodley,[1,3] George N. Ghalanos,[1,4] Andreas Ø. Svela,[1,4] Niall Moroney,[1,4] and Pascal Del'Haye[1,*]

[1]National Physical Laboratory (NPL), Teddington TW11 0LW, UK
[2]City University of London, London, EC1V 0HB, UK
[3]Heriot-Watt University, Edinburgh, EH14 4AS, Scotland, UK
[4]Blackett Laboratory, Imperial College London, SW7 2AZ, UK
*Corresponding author: pascal.delhaye@npl.co.uk

Received 21 September 2018; revised 6 December 2018; accepted 8 January 2019 (Doc. ID 346553); published 19 February 2019

The recent demonstration of dissipative Kerr solitons in microresonators has opened a new pathway for the generation of ultrashort pulses and low-noise frequency combs with gigahertz to terahertz repetition rates, enabling applications in frequency metrology, astronomy, optical coherent communications, and laser-based ranging. A main challenge for soliton generation, in particular in ultra-high-Q resonators, is the sudden change in circulating intracavity power during the onset of soliton generation. This sudden power change requires precise control of the seed laser frequency and power or fast control of the resonator temperature. Here, we report a robust and simple way to increase the soliton access window by using an auxiliary laser that passively stabilizes intracavity power. In our experiments with fused silica resonators, we are able to extend the access range of microresonator solitons by two orders of magnitude, which enables soliton generation by slow and manual tuning of the pump laser into resonance and at unprecedented low power levels. Importantly, this scheme eliminates the sudden change in circulating power ("soliton step") during transition into the soliton regime. Both single- and multi-soliton mode-locked states are generated in a 1.3-mm-diameter fused silica microrod resonator with a free spectral range of ∼50.6 GHz, at a 1554 nm pump wavelength at threshold powers <3 mW. Moreover, with a smaller 230-μm-diameter microrod, we demonstrate soliton generation at 780 μW threshold power. The passive enhancement of the soliton access range paves the way for robust and low-threshold microcomb systems and has the potential to be a practical tool for soliton microcomb generation.

https://doi.org/10.1364/OPTICA.6.000206

1. INTRODUCTION

Over the past two decades, optical frequency combs based on mode-locked lasers have revolutionized the field of precision spectroscopy with an unprecedented frequency measurement precision [1,2]. They have attracted great attention in many areas, such as optical clocks [3,4], ultralow-noise microwave generation [5,6], photonic analog to digital converters (ADCs) and radar [7,8], and gas monitoring [9], just to name a few. Nowadays, Kerr frequency combs ("microcombs") based on parametric four-wave mixing in monolithic high-Q microresonators provide an alternative scheme to miniaturize comb systems and enable out-of-lab applications [10–12]. Microcombs have been demonstrated in resonators made from silica [10,13], magnesium fluoride (MgF_2) [14,15], silicon nitride (Si_3N_4) [16–21], silicon (Si) [22], diamond [23], hydex [24], and several other materials. More recently, dissipative Kerr soliton formation has been observed in microresonators providing low noise, fully coherent Kerr frequency combs with ultrashort optical pulse trains and reproducible spectral envelopes [14] spanning up to more than an octave [21,25]. So far, *soliton* microcombs have been reported in MgF_2 [14,15], Si_3N_4 [18–21], silica [26,27], and Si [28] with repetition rates ranging from 1 THz [21,25] down to 1.8 GHz [29], at wavelengths all the way from the visible [30] to the mid-infrared [28]. Indeed, soliton microcombs have already been successfully used for optical frequency synthesizers [31], astronomy [32,33], optical coherent communications [34], laser-based light detection and ranging [35,36], and dual-comb spectroscopy [37–39]. Moreover, soliton crystals [40] and Raman Stokes solitons [41] have been recently observed in microresonator systems.

The formation of a single soliton in microresonators typically requires the pump frequency to be red-detuned relative to the thermally shifted cavity resonance [14]. However, in most resonators in a steady state (no solitons), red-detuned pump frequencies close to the resonance center are unstable, while blue-detuned frequencies are stable [42–44]. As a result, accessing soliton states is experimentally challenging. To trigger the soliton states, different methods have been developed, such as power kicking [45,46],

frequency kicking [47,48], and thermal control [49]. Direct soliton generation can also be achieved by optimizing laser tuning speed and stopping at the right frequency. This method works in materials with weak thermo-optic effect, such as MgF_2 [14]. Power and frequency kicking methods are based on abrupt changes in the pump power or frequency, respectively. These changes are much faster than the thermal drift of the resonator modes. Recent work in Si_3N_4 and MgF_2 microresonators demonstrated that multi-soliton states can be deterministically switched to single-soliton states by reducing the number of solitons one by one through backward tuning of the pump frequency [20]. Moreover, a nearby mode on the red-detuned side of the pump resonance has been reported to passively stabilize the thermal dynamics of the resonators [21], and recently it has been reported that coupling of counterpropagating light into a resonator mode can help to access soliton states [50,51]. In addition, it has been demonstrated that spatial mode interaction in microresonators has a positive effect on single-soliton generation [52].

A key challenge for most applications using microresonator-based frequency combs is how to easily access soliton states. In this work, we show a detailed study of the passive enhancement of the soliton access range by using an auxiliary laser. The auxiliary laser compensates sudden intracavity power changes when the microresonator enters the soliton regime. Using this method, the length of the soliton steps is extended from 100 kHz to 10 MHz, which enables access to single-soliton states without specific requirements for pump laser tuning speed or power kicking techniques. Soliton states can be reached by arbitrary slow tuning of the laser into resonance, which significantly simplifies the soliton generation process. In particular, this enables access to soliton states in ultrahigh-Q resonators with flawless mode spectra (no mode crossings), which has been previously challenging. The enhanced soliton access range enables us to generate solitons at very low threshold power of 780 μW in a 230-μm-diameter microrod resonator (280 GHz mode spacing). In addition we demonstrate single- and multi-soliton states at 3 mW threshold power in 1.3-mm-diameter glass rods (50 GHz mode spacing). The single-soliton optical spectrum has a smooth, sech^2-like shape without significant imperfections due to mode crossings. Low power consumption of microresonator solitons is particularly important for out-of-the-lab applications of frequency combs, e.g., in battery powered systems [53].

2. PRINCIPLE OF PASSIVE SOLITON STABILIZATION

Figure 1(a) shows the concept of using an auxiliary continuous-wave laser to increase the access range for microresonator solitons. The auxiliary laser at 1.3 μm is kept at a fixed frequency on a resonator mode, while a soliton is generated by a second laser at 1.5 μm. The 1.3 μm laser provides a background signal that compensates for fluctuations of the 1.5 μm soliton laser at time scales slower than the cavity build-up time. At the output, the soliton pulse can be separated using a wavelength division multiplexer (WDM). Figure 1(b) illustrates the intracavity power before and after entering the soliton state. A small portion of the 1.3 μm auxiliary laser power is coupled into the resonator prior to soliton generation. Once the soliton is formed, the intracavity power of the auxiliary laser passively rises to compensate for the temperature variation of the resonator caused by the loss of intracavity pump power. In the soliton state, the intracavity field consists simultaneously of an intense soliton pulse, weak 1.5 μm CW background, and 1.3 μm auxiliary CW background. The resonator used in the experiment is a fused silica microrod resonator, shown in Fig. 1(c) [54] with a Q-factor of 2×10^8 at 1.3 μm and 3.7×10^8 at 1.5 μm. By controlling the curvature of the resonator sidewalls during CO_2 laser machining, the microrod resonator can be engineered to have an ultrahigh optical Q-factor and minimal avoided crossings between different mode families.

Figures 1(d)–1(f) show how the auxiliary laser stabilizes the optically circulating power within the resonator to enhance soliton access range. First, the frequency of the 1.3 μm auxiliary laser is tuned into a high-Q optical resonator mode from the blue side and fixed on the blue side of the resonance, as shown in Fig. 1(d). Due to absorption of light, the resonator heats up, red-shifting the resonances at 1.3 μm and 1.5 μm. Note that the mode at 1.3 μm resonance shifts by a factor of $1.16 = \Delta f_{1330}/\Delta f_{1550}$ more than the 1.5 μm resonance as a result of the higher mode number. The 1.5 μm pump laser is now tuned into its resonance from the blue side, passing through a chaotic four-wave mixing regime. The rising intracavity pump power has the same thermal effect as the 1.3 μm auxiliary laser and also red-shifts both resonances [shown in Fig. 1(e)]. This red shift of the resonances at 1.3 μm causes the 1.3 μm intracavity power to decrease, counteracting the temperature rise induced by the 1.5 μm pump laser. The temperature (and intracavity optical powers) of the microresonator will reach a stable equilibrium, since the frequencies of both lasers are on the blue side of their optical resonance modes [42]. The intracavity power of the 1.3 μm auxiliary laser will be further reduced as the 1.5 μm pump laser scans into the resonance [from t_0 to t_1 in Fig. 1(g)]. Once the pump laser gets close to zero detuning, the resonator abruptly transitions into the soliton regime. In this regime, the pump resonance splits into a soliton resonance and a cavity resonance [20]. As shown in Fig. 1(f), the low-frequency, small peak is the soliton-induced "S-resonance." Upon entering the soliton regime, the intracavity pump power decreases abruptly, blue-shifting the resonances. As a result, the intracavity auxiliary power passively rises to stabilize the temperature of the resonator [from t_1 to t_2 in Fig. 1(g)]. Figure 1(h) shows the intracavity power (measured by the loss in transmission) when fixing the frequency of the 1.3 μm auxiliary laser on the blue detuned side of its resonance while simultaneously tuning the 1.5 μm pump laser into the pump resonance. We indeed see the 1.3 μm laser compensating for intracavity pump power variation, keeping the total circulating power inside the resonator stable, therefore passively stabilizing the temperature of the microresonator. This effect can be optimized by varying the parameters (optical power and frequency detuning from the resonance) of the 1.3 μm laser, allowing the effective thermal response of silica resonators to be reduced by two orders of magnitude. An animation of the concept is shown in Visualization 1.

3. EXPERIMENTAL SETUP

Figure 2(a) shows the schematic of the experimental setup. A 1.5 μm external cavity diode laser (ECDL) with a short-term linewidth of <10 kHz is used as the pump laser for generating a soliton frequency comb. A 1.3 μm ECDL is used as an auxiliary laser to compensate changes in the circulating power in the resonator. As mentioned above, as well as choosing a high-Q mode family with minimal avoided crossings for soliton generation, we also choose a high-Q optical mode at 1334 nm, which enables us to operate the auxiliary laser at a low power level similar to the pump

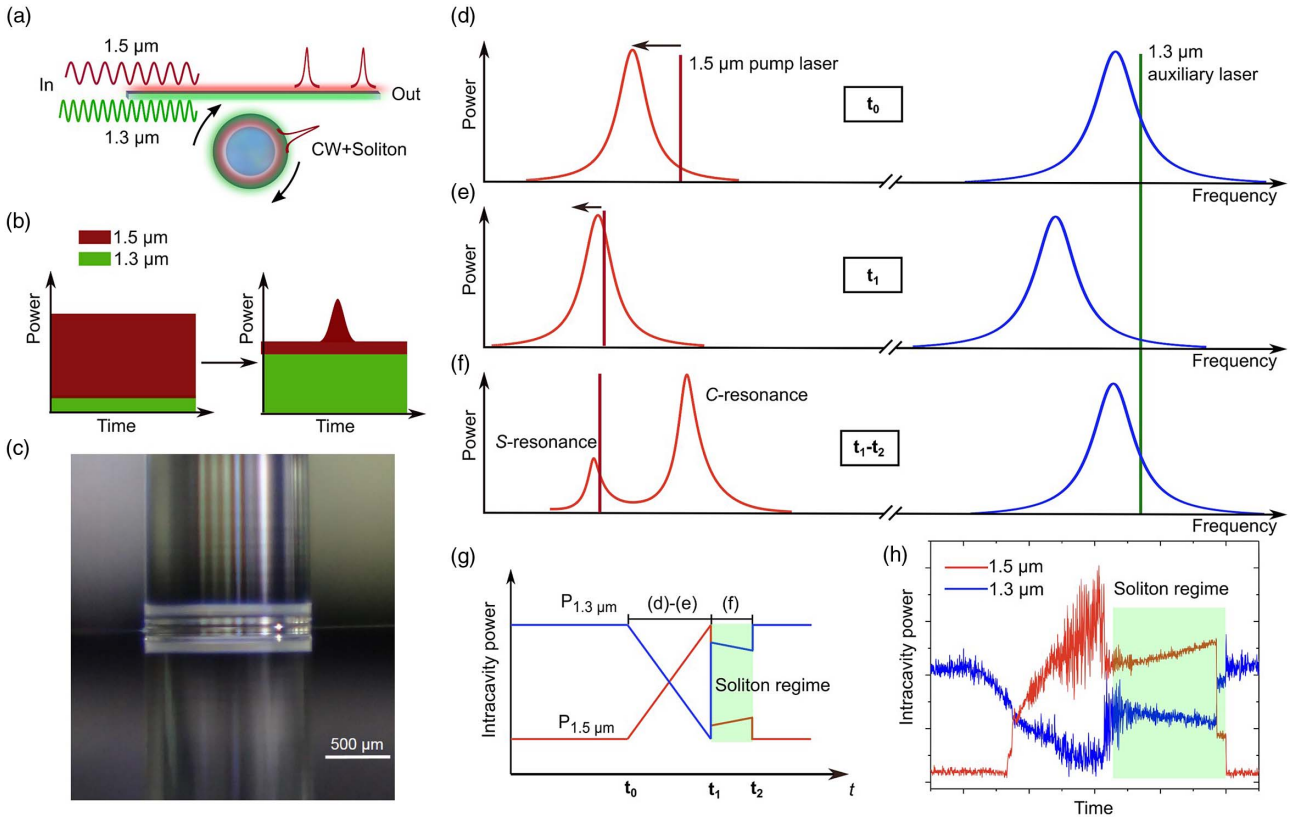

Fig. 1. (a) Scheme of using an auxiliary laser to assist in accessing soliton states. The 1.5 μm pump laser generates a microresonator soliton while the second laser at 1.3 μm wavelength passively stabilizes the intracavity power. (b) Illustration of the intracavity power (red: 1.5 μm, green: 1.3 μm) before (left panel) and after (right panel) soliton generation. (c) Microscope image of the 1.3-mm-diameter fused silica microrod resonator used in the experiments. Panels (d)–(f) show the principle of the passive compensation of the circulating power in the microresonator by the auxiliary laser in order to enhance the soliton range (animated version available in Visualization 1). In panel (d), only the auxiliary laser is coupled into a resonator mode. When tuning the pump laser into resonance, shown in panel (e), the thermal shift of the resonator modes automatically reduces the amount of light coupled into the auxiliary resonator mode. Panel (f) shows the abrupt transition into a soliton state, which reduces the coupled power of the pump laser. In this state, the pump resonance splits into C-resonance (resonance for light arriving out-of-sync with the soliton) and S-resonance (resonance for light arriving in-sync with the soliton). The reduction in pump power in the soliton regime moves the auxiliary resonance back towards the auxiliary laser and thus compensates the power loss. Panel (g) shows the temporal evolution of the intracavity power when tuning the pump laser into resonance with a fixed frequency auxiliary laser. Panel (h) shows a measurement according to the scheme in panel (g). The two steps in soliton regime correspond to different soliton numbers circulating in the cavity. The 1.3 μm auxiliary laser passively compensates changes in circulating power of the pump laser.

laser power. The two lasers are combined with a WDM and evanescently coupled to the microresonator via a tapered optical fiber. Two fiber polarization controllers (PCs) are used to optimize the coupling efficiency of the auxiliary and pump light into the microresonator. As shown in Fig. 1(c), a 1.3-mm-diameter microrod resonator is used for soliton generation with a free spectral range (FSR) of 50.6 GHz. The optical modes used to generate the soliton frequency comb have a Q-factor of 3.7×10^8 with a ~520 kHz linewidth (measured at 1554 nm), while the chosen auxiliary optical mode has a Q-factor of 2×10^8 with a ~1.1 MHz linewidth (measured at 1334 nm). At the resonator output, the auxiliary and pump lights are separated by another WDM. One part of the 1.5 μm light is sent to an optical spectrum analyzer (OSA), and the rest is sent into a fiber Bragg grating notch filter to separate the generated comb light from the pump light. The comb light is sent to two photodetectors: one for monitoring the comb power (PD1), and the other (PD2) with a 50 GHz bandwidth for detecting the repetition rate of the generated soliton frequency comb on an electronic spectrum analyzer (ESA). The auxiliary light is monitored by a third photodiode (PD3).

By optimizing the optical power of the 1334 nm auxiliary laser and its detuning from the optical resonance, both multi- and single-soliton states can be accessed by manually forward-tuning the pump laser into the soliton steps. If a multi-soliton emerges first, a single soliton can be generated by further forward-tuning the pump frequency. Figure 2(b) shows the optical spectrum of a single soliton at a pump power of ~80 mW, while ~60 mW of 1334 nm auxiliary power is used to compensate for the thermal effect. Note that during the experiments, the auxiliary laser is free running without feedback control on the laser frequency or the power. Thermal self-locking of the resonator to the auxiliary laser ensures that the detuning of the auxiliary laser remains largely unaffected by laser frequency drifts. The optical spectrum of the single soliton has a smooth, sech^2-like shape [red dashed line in Fig. 2(b)]. Note that there is no significant avoided-crossing

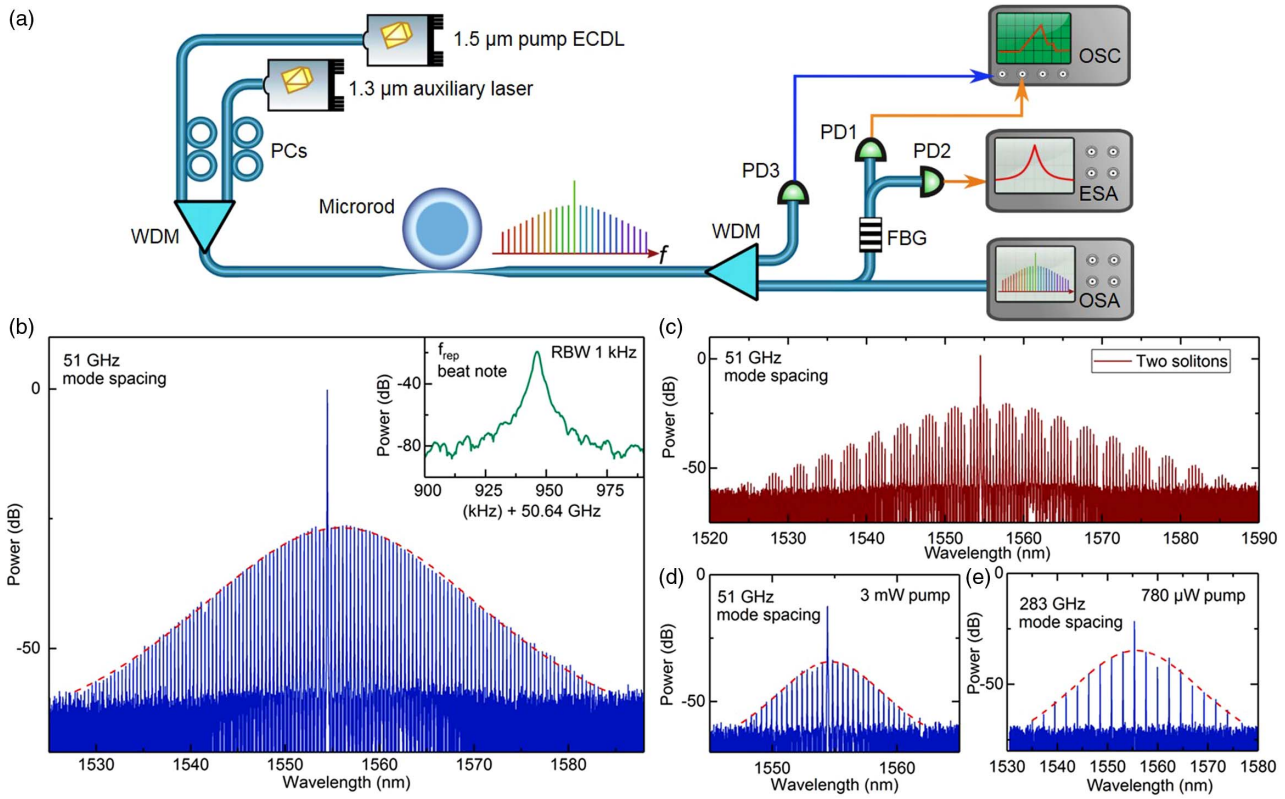

Fig. 2. (a) Experimental setup for the generation of a soliton mode-locked frequency comb in a silica microrod resonator by using an auxiliary laser to compensate the resonator's thermal shift. ECDL, external cavity diode laser; WDM, wavelength division multiplexer; PC, polarization controller; FBG, fiber Bragg grating; PD, photodetector; OSC, oscilloscope; OSA, optical spectrum analyzer; ESA, electronic spectrum analyzer. (b) Optical spectrum of a single-soliton state pumped with 80 mW optical power compensated by 60 mW auxiliary laser power. The red dashed line shows the fitted sech^2 envelope. Inset: spectrum of the microwave repetition rate f_{rep} of the single-soliton state measured with a 1 kHz resolution bandwidth (RBW). (c) Optical spectrum of a two-soliton state pumped with the same settings of pump and auxiliary laser as Fig. 2(b). (d) Optical spectrum of a single-soliton state pumped at 3 mW power with a fitted sech^2 envelope. (e) Optical spectrum of a single-soliton state in a 230-μm-diameter microrod pumped with 780 μW power.

behavior visible in the spectrum range. The 3 dB bandwidth of the spectrum is around 1.3 THz, corresponding to a 240 fs optical pulse. Once excited, the soliton states can survive for >3 h without active feedback locking. For longer soliton lifetimes, active feedback locking can be used [46]. The soliton state is further confirmed by measuring the RF spectrum at the comb's 50.6 GHz repetition rate (f_{rep}). The beat note from the PD is amplified and mixed down to 13.6 GHz with a 37 GHz microwave signal from a signal generator. The down-converted spectrum at 13.6 GHz is analyzed with an ESA. The inset in Fig. 2(b) shows the f_{rep} beat note when the microcomb is in the single-soliton state. Figure 2(c) shows the optical spectrum of a two-soliton state at a pump power of ~80 mW with the same auxiliary laser settings as the (optical power and detuning) as Fig. 2(b). The demonstrated technique constitutes a simple and robust way to access single solitons in microresonators, making the system insensitive to pump laser frequency and power fluctuations. In particular, this technique enables accessing soliton states in resonators without mode crossings that naturally exhibit very narrow soliton steps.

To explore the full advantages of our proposed technique, we obtain a single-soliton frequency comb with both the pump laser and auxiliary laser operating at very low optical powers. Figure 2(d) shows the optical spectrum of a single-soliton state pumped by 3 mW optical power at 1554 nm with 2.5 mW at 1334 nm auxiliary laser for compensating for the thermal effect. The spectrum has a smooth sech^2-like shape (red dashed line). In addition, using a smaller diameter (230 μm) microrod, a single-soliton state is accessed with 780 μW optical power (pump power in the tapered optical fiber), as shown in Fig. 2(e). To the best of our knowledge, this is the first demonstration of a soliton microcomb at sub-mW power levels [53].

4. ENHANCEMENT OF THE SOLITON ACCESS RANGE

Soliton mode-locked states are generated by scanning the pump laser frequency from blue detuning to red detuning with respect to the resonator mode. Due to thermally induced (and Kerr effect induced) resonance frequency shifts, the measured power of the generated comb modes has a triangular shape [42]. This is shown in the upper panel in Fig. 3(a) for a measurement without the auxiliary laser. The pump wavelength, optical power, and laser scan speed are ~1554 nm, ~20 mW, and ~35 MHz/ms, respectively. The width of the broadened resonance is ~700 MHz. At the end of the triangle shape (marked with a dash circle), "step-like" features are observable, which indicate the presence of soliton states. The inset in the upper panel in Fig. 3(a) shows a zoom into a single-soliton step without the auxiliary laser with a width of ~100 kHz (corresponding to a few microseconds for the used laser sweep speed). The sudden temperature change in the resonator after

soliton transition prevents the stable generation of solitons by simply stopping the laser frequency tuning within the step.

In contrast, the lower panel in Fig. 3(a) shows the microresonator resonance when the 1334 nm auxiliary laser with 50 mW optical power is simultaneously coupled into the resonator. The 1554 nm pump laser is operated at the same parameters (laser scan speed and optical power) as in the measurement without the auxiliary laser. With the auxiliary laser coupled into the

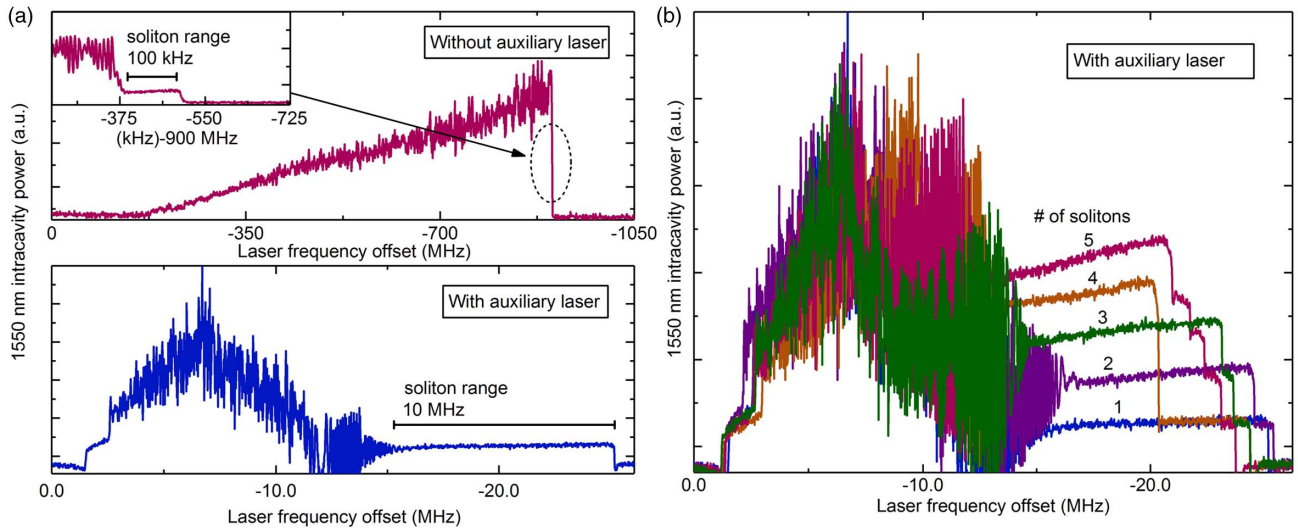

Fig. 3. Enhancement of the soliton access range. (a) Experimental traces of the 1550 nm intracavity power when scanning the pump laser frequency from blue to red detuning without auxiliary laser (upper panel) and with auxiliary laser (lower panel). The laser tuning speed is ~35 MHz/ms. The inset in the upper panel shows a trace of the narrow soliton step with a width of ~100 kHz without auxiliary laser. The lower panel shows the same resonance while 50 mW auxiliary power is coupled into the resonator. The thermally broadened width of the resonance is reduced, while the soliton access range is increased by two orders of magnitude to ~10 MHz. The presence of the auxiliary laser eliminates the sudden power change ("soliton step") during the transition into the soliton regime. (b) Traces of the 1550 nm intracavity power for different multi-soliton states (with auxiliary laser).

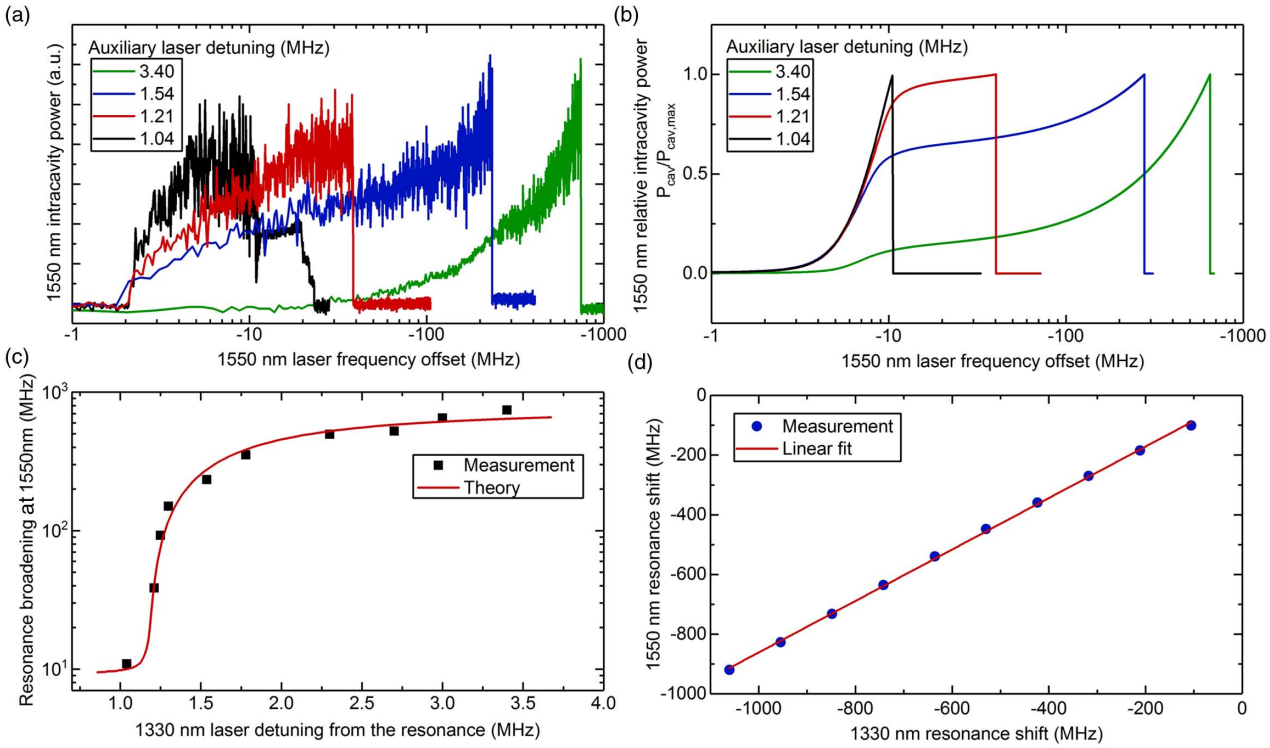

Fig. 4. Tuning behavior of the doubly pumped resonator system. (a) (b) Experimental and numerically calculated traces of the shape of the thermally broadened resonances at 1550 nm at different fixed detunings of the 1330 nm laser from the auxiliary resonance. The 1550 nm pump laser is tuned at ~35 MHz/ms during the measurement. (c) Experimental measurement (squares) of the width of 1550 nm resonances as a function of the detuning of the 1330 nm auxiliary laser from its resonance. The red line is a simulation based on the thermal dynamic behavior of a doubly pumped microresonator. (d) Experimental measurement and linear fit of the relative resonance shift of the 1550 nm and 1330 nm modes with a slope of 0.862.

resonator, the length of the single-soliton step is significantly increased by two orders of magnitude to more than 10 MHz. Note that the overall width of the thermally broadened resonance is reduced to ∼25 MHz, such that the soliton regime spans nearly half the resonance frequency range. The overall procedure using the auxiliary laser to reduce thermal broadening and extend the soliton range is presented in Supplement 1. Figure 3(b) shows repeated measurements with examples of different soliton steps at 1554 nm when the auxiliary laser is close to its resonance. Each step represents a different integer number of solitons circulating inside the resonator. Note that, with the auxiliary laser, the length of soliton steps in time depends on laser scanning speed, instead of thermal relaxation velocity. As a result, when scanning more slowly (∼1 MHz/ms), the soliton steps can last for even tens of milliseconds, which is four orders longer than that without the auxiliary laser. Figure 4(a) shows the influence of the auxiliary laser detuning from its resonance on the thermally broadened width of the 1554 nm resonance when 20 mW pump and 50 mW auxiliary power are coupled into the resonator. During this measurement, the auxiliary resonance thermally stabilizes itself to the auxiliary laser. It can be seen that smaller detuning of the auxiliary laser leads to a better stabilization of the circulating intracavity power and thus a reduced thermal broadening effect at 1554 nm resonance. A mathematical description of the narrowing can be found in Supplement 1. Figure 4(b) shows the numerical calculations, based on the dynamical thermal behavior (the Kerr effect is not included here) of the microresonator resonance in the presence of an auxiliary laser in a second resonance. The results are consistent with the experimental measurements in Fig. 4(a). Figure 4(c) shows both the experimentally measured and the numerically calculated width of the 1554 nm resonance as a function of the detuning of the 1334 nm laser from the auxiliary resonance (using the same power as the pump and auxiliary laser). More details about Fig. 4(c) are presented in Supplement 1 along with a laser detuning versus optical power map of the auxiliary laser.

All the previous calculations take into account a larger thermally induced resonance frequency shift of the mode at 1334 nm as a result of the higher mode number. We verify this by measuring the relative resonance shift of pump resonance and auxiliary resonance when heating up the resonator with one of the lasers (see Supplement 1 for more details). The results are displayed in Fig. 4(d) and show a slope of $\Delta f_{1550}/\Delta f_{1330} = 0.862$, which is close to the expected value of 0.859 based on the ratio of the mode numbers. This larger resonance shift at 1.3 μm gives the auxiliary laser more leverage on the resonator temperature and enables its operation at reduced power compared to the pump laser.

5. CONCLUSION

In summary, we have demonstrated that the soliton access range of microresonator-based frequency combs can be greatly enhanced by coupling an auxiliary laser into a second high-Q resonance. This increases the laser frequency range in which a microresonator generates Kerr solitons by two orders of magnitude and significantly reduces the sensitivity of microcomb states to pump laser frequency and power fluctuations. The scheme provides "step-free" access to microresonator solitons by eliminating the sudden power change during soliton transition. This enables slow and manual tuning of the pump laser to generate soliton frequency combs. The enhanced soliton access range allows us to demonstrate the first microresonator solitons at sub-mW power levels, which is important for future fully chip integrated microcomb systems. In addition, the auxiliary laser could be used as an active actuator to stabilize a soliton frequency comb as shown in Ref. [55]. We believe that our technique of passively stabilizing microresonator mode spectra could be applied to other resonator systems/applications that require insensitivity to perturbations by an external laser.

Note: we would like to draw the readers' attention to the following related preprints: Refs. [56,57].

Funding. H2020 European Research Council (ERC) (756966, CounterLight); H2020 Marie Skłodowska-Curie Actions (MSCA) (CoLiDR, 748519; GA-2015-713694); Engineering and Physical Sciences Research Council (EPSRC) (CDT for Applied Photonics); National Physical Laboratory (NPL) (Strategic Research).

Acknowledgment. LDB and MTMW acknowledge funding from the EPSRC via the CDT for Applied Photonics. AS acknowledges funding from Aker Scholarship.

See Supplement 1 for supporting content.

REFERENCES

1. T. Rosenband, D. B. Hume, P. O. Schmidt, C. W. Chou, A. Brusch, L. Lorini, W. H. Oskay, R. E. Drullinger, T. M. Fortier, J. E. Stalnaker, S. A. Diddams, W. C. Swann, N. R. Newbury, W. M. Itano, D. J. Wineland, and J. C. Bergquist, "Frequency ratio of Al+ and Hg+ single-ion optical clocks; metrology at the 17th decimal place," Science **319**, 1808–1812 (2008).
2. C. W. Chou, D. B. Hume, J. C. Koelemeij, D. J. Wineland, and T. Rosenband, "Frequency comparison of two high-accuracy Al+ optical clocks," Phys. Rev. Lett. **104**, 070802 (2010).
3. S. A. Diddams, T. Udem, J. C. Bergquist, E. A. Curtis, R. E. Drullinger, L. Hollberg, W. M. Itano, W. D. Lee, C. W. Oates, K. R. Vogel, and D. J. Wineland, "An optical clock based on a single trapped 199Hg+ ion," Science **293**, 825–828 (2001).
4. N. R. Newbury, "Searching for applications with a fine-tooth comb," Nat. Photonics **5**, 186–188 (2011).
5. T. M. Fortier, M. S. Kirchner, F. Quinlan, J. Taylor, J. C. Bergquist, T. Rosenband, N. Lemke, A. Ludlow, Y. Jiang, C. W. Oates, and S. A. Diddams, "Generation of ultrastable microwaves via optical frequency division," Nat. Photonics **5**, 425–429 (2011).
6. X. Xie, R. Bouchand, D. Nicolodi, M. Giunta, W. Hänsel, M. Lezius, A. Joshi, S. Datta, C. Alexandre, and M. Lours, "Photonic microwave signals with zeptosecond-level absolute timing noise," Nat. Photonics **11**, 44–47 (2017).
7. J. Kim, M. J. Park, M. H. Perrott, and F. X. Kärtner, "Photonic subsampling analog-to-digital conversion of microwave signals at 40-GHz with higher than 7-ENOB resolution," Opt. Express **16**, 16509–16515 (2008).
8. P. Ghelfi, F. Laghezza, F. Scotti, G. Serafino, A. Capria, S. Pinna, D. Onori, C. Porzi, M. Scaffardi, and A. Malacarne, "A fully photonics-based coherent radar system," Nature **507**, 341–345 (2014).
9. G. B. Rieker, F. R. Giorgetta, W. C. Swann, J. Kofler, A. M. Zolot, L. C. Sinclair, E. Baumann, C. Cromer, G. Petron, and C. Sweeney, "Frequency-comb-based remote sensing of greenhouse gases over kilometer air paths," Optica **1**, 290–298 (2014).
10. P. Del'Haye, A. Schliesser, O. Arcizet, T. Wilken, R. Holzwarth, and T. J. Kippenberg, "Optical frequency comb generation from a monolithic microresonator," Nature **450**, 1214–1217 (2007).
11. T. J. Kippenberg, R. Holzwarth, and S. A. Diddams, "Microresonator-based optical frequency combs," Science **332**, 555–559 (2011).
12. T. J. Kippenberg, A. L. Gaeta, M. Lipson, and M. L. Gorodetsky, "Dissipative Kerr solitons in optical microresonators," Science **361**, eaan8083 (2018).
13. J. Li, H. Lee, T. Chen, and K. J. Vahala, "Low-pump-power, low-phase-noise, and microwave to millimeter-wave repetition rate operation in microcombs," Phys. Rev. Lett. **109**, 233901 (2012).

14. T. Herr, V. Brasch, J. D. Jost, C. Y. Wang, N. M. Kondratiev, M. L. Gorodetsky, and T. J. Kippenberg, "Temporal solitons in optical microresonators," Nat. Photonics **8**, 145–152 (2014).
15. W. Liang, D. Eliyahu, V. S. Ilchenko, A. A. Savchenkov, A. B. Matsko, D. Seidel, and L. Maleki, "High spectral purity Kerr frequency comb radio frequency photonic oscillator," Nat. Commun. **6**, 7957 (2015).
16. M. A. Foster, J. S. Levy, O. Kuzucu, K. Saha, M. Lipson, and A. L. Gaeta, "Silicon-based monolithic optical frequency comb source," Opt. Express **19**, 14233–14239 (2011).
17. S.-W. Huang, J. Yang, J. Lim, H. Zhou, M. Yu, D.-L. Kwong, and C. Wong, "A low-phase-noise 18 GHz Kerr frequency microcomb phase-locked over 65 THz," Sci. Rep. **5**, 13355 (2015).
18. V. Brasch, M. Geiselmann, T. Herr, G. Lihachev, M. H. Pfeiffer, M. L. Gorodetsky, and T. J. Kippenberg, "Photonic chip-based optical frequency comb using soliton Cherenkov radiation," Science **351**, 357–360 (2016).
19. P.-H. Wang, J. A. Jaramillo-Villegas, Y. Xuan, X. Xue, C. Bao, D. E. Leaird, M. Qi, and A. M. Weiner, "Intracavity characterization of micro-comb generation in the single-soliton regime," Opt. Express **24**, 10890–10897 (2016).
20. H. Guo, M. Karpov, E. Lucas, A. Kordts, M. H. Pfeiffer, V. Brasch, G. Lihachev, V. E. Lobanov, M. L. Gorodetsky, and T. J. Kippenberg, "Universal dynamics and deterministic switching of dissipative Kerr solitons in optical microresonators," Nat. Phys. **13**, 94–102 (2017).
21. Q. Li, T. C. Briles, D. A. Westly, T. E. Drake, J. R. Stone, B. R. Ilic, S. A. Diddams, S. B. Papp, and K. Srinivasan, "Stably accessing octave-spanning microresonator frequency combs in the soliton regime," Optica **4**, 193–203 (2017).
22. A. G. Griffith, R. K. Lau, J. Cardenas, Y. Okawachi, A. Mohanty, R. Fain, Y. H. D. Lee, M. Yu, C. T. Phare, and C. B. Poitras, "Silicon-chip mid-infrared frequency comb generation," Nat. Commun. **6**, 6299 (2015).
23. B. Hausmann, I. Bulu, V. Venkataraman, P. Deotare, and M. Lončar, "Diamond nonlinear photonics," Nat. Photonics **8**, 369–374 (2014).
24. M. Peccianti, A. Pasquazi, Y. Park, B. Little, S. T. Chu, D. Moss, and R. Morandotti, "Demonstration of a stable ultrafast laser based on a nonlinear microcavity," Nat. Commun. **3**, 765 (2012).
25. M. H. Pfeiffer, C. Herkommer, J. Liu, H. Guo, M. Karpov, E. Lucas, M. Zervas, and T. J. Kippenberg, "Octave-spanning dissipative Kerr soliton frequency combs in Si_3N_4 microresonators," Optica **4**, 684–691 (2017).
26. X. Yi, Q.-F. Yang, K. Y. Yang, M.-G. Suh, and K. Vahala, "Soliton frequency comb at microwave rates in a high-Q silica microresonator," Optica **2**, 1078–1085 (2015).
27. E. Obrzud, S. Lecomte, and T. Herr, "Temporal solitons in microresonators driven by optical pulses," Nat. Photonics **11**, 600–607 (2017).
28. M. Yu, Y. Okawachi, A. G. Griffith, M. Lipson, and A. L. Gaeta, "Mode-locked mid-infrared frequency combs in a silicon microresonator," Optica **3**, 854–860 (2016).
29. M.-G. Suh and K. Vahala, "Gigahertz-repetition-rate soliton microcombs," Optica **5**, 65–66 (2018).
30. S. H. Lee, D. Y. Oh, Q.-F. Yang, B. Shen, H. Wang, K. Y. Yang, Y.-H. Lai, X. Yi, X. Li, and K. Vahala, "Towards visible soliton microcomb generation," Nat. Commun. **8**, 1295 (2017).
31. D. T. Spencer, T. Drake, T. C. Briles, J. Stone, L. C. Sinclair, C. Fredrick, Q. Li, D. Westly, B. R. Ilic, and A. Bluestone, "An optical-frequency synthesizer using integrated photonics," Nature **557**, 81–85 (2018).
32. E. Obrzud, M. Rainer, A. Harutyunyan, M. Anderson, M. Geiselmann, B. Chazelas, S. Kundermann, S. Lecomte, M. Cecconi, and A. Ghedina, "A microphotonic astrocomb," arXiv:1712.09526 (2017).
33. M.-G. Suh, X. Yi, Y.-H. Lai, S. Leifer, I. S. Grudinin, G. Vasisht, E. C. Martin, M. P. Fitzgerald, G. Doppmann, and J. Wang, "Searching for exoplanets using a microresonator astrocomb," arXiv:1801.05174 (2018).
34. J. Pfeifle, V. Brasch, M. Lauermann, Y. Yu, D. Wegner, T. Herr, K. Hartinger, P. Schindler, J. Li, and D. Hillerkuss, "Coherent terabit communications with microresonator Kerr frequency combs," Nat. Photonics **8**, 375–380 (2014).
35. M.-G. Suh and K. J. Vahala, "Soliton microcomb range measurement," Science **359**, 884–887 (2018).
36. P. Trocha, M. Karpov, D. Ganin, M. H. Pfeiffer, A. Kordts, S. Wolf, J. Krockenberger, P. Marin-Palomo, C. Weimann, and S. Randel, "Ultrafast optical ranging using microresonator soliton frequency combs," Science **359**, 887–891 (2018).
37. M.-G. Suh, Q.-F. Yang, K. Y. Yang, X. Yi, and K. J. Vahala, "Microresonator soliton dual-comb spectroscopy," Science **354**, 600–603 (2016).
38. A. Dutt, C. Joshi, X. Ji, J. Cardenas, Y. Okawachi, K. Luke, A. L. Gaeta, and M. Lipson, "On-chip dual-comb source for spectroscopy," Sci. Adv. **4**, e1701858 (2018).
39. M. Yu, Y. Okawachi, A. G. Griffith, N. Picqué, M. Lipson, and A. L. Gaeta, "Silicon-chip-based mid-infrared dual-comb spectroscopy," Nat. Commun. **9**, 1869 (2018).
40. D. C. Cole, E. S. Lamb, P. Del'Haye, S. A. Diddams, and S. B. Papp, "Soliton crystals in Kerr resonators," Nat. Photonics **11**, 671–676 (2017).
41. Q.-F. Yang, X. Yi, K. Y. Yang, and K. Vahala, "Stokes solitons in optical microcavities," Nat. Phys. **13**, 53–57 (2017).
42. T. Carmon, L. Yang, and K. J. Vahala, "Dynamical thermal behavior and thermal self-stability of microcavities," Opt. Express **12**, 4742–4750 (2004).
43. Z. Kang, F. Li, J. Yuan, K. Nakkeeran, J. N. Kutz, Q. Wu, C. Yu, and P. Wai, "Deterministic generation of single soliton Kerr frequency comb in microresonators by a single shot pulsed trigger," Opt. Express **26**, 18563–18577 (2018).
44. X. Sun, R. Luo, X. C. Zhang, and Q. Lin, "Squeezing the fundamental temperature fluctuations of a high-Q microresonator," Phys. Rev. A **95**, 023822 (2017).
45. V. Brasch, M. Geiselmann, M. H. Pfeiffer, and T. J. Kippenberg, "Bringing short-lived dissipative Kerr soliton states in microresonators into a steady state," Opt. Express **24**, 29312–29320 (2016).
46. X. Yi, Q.-F. Yang, K. Y. Yang, and K. Vahala, "Active capture and stabilization of temporal solitons in microresonators," Opt. Lett. **41**, 2037–2040 (2016).
47. J. R. Stone, T. C. Briles, T. E. Drake, D. T. Spencer, D. R. Carlson, S. A. Diddams, and S. B. Papp, "Thermal and nonlinear dissipative-soliton dynamics in Kerr-microresonator frequency combs," Phys. Rev. Lett. **121**, 063902 (2018).
48. N. Volet, X. Yi, Q. F. Yang, E. J. Stanton, P. A. Morton, K. Y. Yang, K. J. Vahala, and J. E. Bowers, "Micro-resonator soliton generated directly with a diode laser," Laser Photon. Rev. **12**, 1700307 (2018).
49. C. Joshi, J. K. Jang, K. Luke, X. Ji, S. A. Miller, A. Klenner, Y. Okawachi, M. Lipson, and A. L. Gaeta, "Thermally controlled comb generation and soliton modelocking in microresonators," Opt. Lett. **41**, 2565–2568 (2016).
50. Y. Geng, M. Liao, H. Zhou, B. Wu, and K. Qiu, "Kerr frequency comb dynamics circumventing cavity thermal behavior," in *Nonlinear Optics* (Optical Society of America, 2017), paper NM1A. 4.
51. Y. Geng, X. Huang, W. Cui, Y. Ling, B. Xu, J. Zhang, X. Yi, B. Wu, S.-W. Huang, and K. Qiu, "Terabit optical OFDM superchannel transmission via coherent carriers of a hybrid chip-scale soliton frequency comb," Opt. Lett. **43**, 2406–2409 (2018).
52. C. Bao, Y. Xuan, D. E. Leaird, S. Wabnitz, M. Qi, and A. M. Weiner, "Spatial mode-interaction induced single soliton generation in microresonators," Optica **4**, 1011–1015 (2017).
53. B. Stern, X. Ji, Y. Okawachi, A. L. Gaeta, and M. Lipson, "Battery-operated integrated frequency comb generator," Nature **562**, 401–405 (2018).
54. P. Del'Haye, S. A. Diddams, and S. B. Papp, "Laser-machined ultra-high-Q microrod resonators for nonlinear optics," Appl. Phys. Lett. **102**, 221119 (2013).
55. J. Jost, E. Lucas, T. Herr, C. Lecaplain, V. Brasch, M. Pfeiffer, and T. Kippenberg, "All-optical stabilization of a soliton frequency comb in a crystalline microresonator," Opt. Lett. **40**, 4723–4726 (2015).
56. Z. Lu, W. Wang, W. Zhang, S. T. Chu, B. E. Little, M. Liu, L. Wang, C.-L. Zou, C.-H. Dong, and B. Zhao, "Deterministic generation and switching of dissipative Kerr soliton in a thermally controlled micro-resonator," arXiv:1810.04983 (2018).
57. R. Niu, S. Wan, S.-M. Sun, T.-G. Ma, H.-J. Chen, W.-Q. Wang, Z.-Z. Lu, W.-F. Zhang, G.-C. Guo, and C.-L. Zou, "Repetition rate tuning of soliton in microrod resonators," arXiv:1809.06490 (2018).